Appl. Phys. B (2017) 123:102
DOI 10.1007/s00340-017-6655-5

**Applied Physics B**
**Lasers and Optics**

# $T^3$-Interferometer for atoms

**M. Zimmermann[1] · M. A. Efremov[1] · A. Roura[1] · W. P. Schleich[1,2] · S. A. DeSavage[3] · J. P. Davis[4] · A. Srinivasan[5] · F. A. Narducci[3] · S. A. Werner[6] · E. M. Rasel[7]**

Received: 6 September 2016 / Accepted: 29 January 2017


**Abstract** The quantum mechanical propagator of a massive particle in a linear gravitational potential derived already in 1927 by Kennard [2, 3] contains a phase that scales with the third power of the time $T$ during which the particle experiences the corresponding force. Since in conventional atom interferometers the internal atomic states are all exposed to the same acceleration $a$, this $T^3$-phase cancels out and the interferometer phase scales as $T^2$. In contrast, by applying an external magnetic field we prepare two different accelerations $a_1$ and $a_2$ for two internal states of the atom, which translate themselves into two different cubic phases and the resulting interferometer phase scales as $T^3$. We present the theoretical background for, and summarize our progress towards experimentally realizing such a novel atom interferometer.

Our proposal of a $T^3$-interferometer for atoms was inspired by the seminal experiment of Hänsch and collaborators [1] to test the equivalence principle of general relativity based on a matter-wave interferometer for two different isotopes of rubidium. Whereas Ref. [1] profits from quadratic phases reminiscent of the Talbot effect we employ the cubic phase of the quantum mechanical propagator associated with a particle moving in a linear potential combined with a Ramsey interferometer. It is with great pleasure that we dedicate this article to Theodor W. Hänsch on the occasion of his 75th birthday.

This article is part of the topical collection “Enlightening the World with the Laser” - Honoring T. W. Hänsch guest edited by Tilman Esslinger, Nathalie Picqué, and Thomas Udem.

✉ M. A. Efremov
max.efremov@gmail.com

1 Institut für Quantenphysik and Center for Integrated Quantum Science and Technology (IQST), Universität Ulm, D-89081 Ulm, Germany

2 Texas A & M University Institute for Advanced Study (TIAS), Institute for Quantum Science and Engineering (IQSE) and Department of Physics and Astronomy, Texas A & M University, College Station, TX 77843-4242, USA

3 Naval Air Systems Command, EO Sensors Division, Patuxent River, MD 20670, USA

4 AMPAC, North Wales, PA 19154, USA

5 St. Mary’s College of Maryland, St. Mary’s City, MD 20686-3001, USA

6 Physics Laboratory, NIST, Gaithersburg, MD 20899, USA

7 Institut für Quantenoptik, Leibniz Universität Hannover, D-30167 Hannover, Germany

## 1 Introduction

Phases play an extraordinary role in quantum theory. On one hand, they represent the central ingredient of wave mechanics à la Schrödinger, and on the other, they build a bridge to classical mechanics à la Hamilton–Jacobi [4]. For these reasons they constitute a crucial ingredient of matter-wave interferometers [5–7] which nowadays represent standard tools for precision measurements. In this article, we propose a new type of atom interferometer whose phase scales with the cube of the time $T$ the atom spends in the interferometer.

### 1.1 In a nutshell

In 1927, Kennard [2, 3] showed that a particle exposed for a time $T$ to a linear potential accumulates a phase proportional to $T^3$. Since then the Kennard phase has been rediscovered by many authors [8–10], especially in the context [11] of atom interferometry. However, no suggestion for its measurement in this field has been given.

It is interesting that recently an experiment [12] on an atom interferometer displaying a cubic phase [13] was reported. Our proposal is different in three aspects: (*i*) We obtain a closed interferometer with four rather than three pulses, and no momentum transfer from the laser beams to the atoms is required. (*ii*) In contrast to Ref. [12] our interferometer relies solely on the application of time-independent forces, and (*iii*) the interferometer of Ref. [12] leads to a phase shift that is quadratic *and* cubic in $T$, whereas the one in our device is solely cubic in $T$, and is proportional to the difference of the squares of these two constant accelerations.

Our scheme is reminiscent of the Ramsey–Bordé interferometer [14, 15] and other four-pulse configurations frequently employed as gradiometers and gyrometers [16–28]. However, we emphasize that in our setup there is no exchange of photon momenta.

In atom interferometry cubic phases are not rare. They appear for example as corrections due to gravity gradients [29–31], but also in the butterfly interferometer which is sensitive to rotation [27, 28]. However, again these devices rely on the exchange of the photon momentum.

There exist many different techniques to calculate the phase shift in an atom interferometer ranging from the semi-classical action [11] associated with the Feynman path integral [8], via the intriguing formalism of Christian Bordé based on a five-dimensional theory [7, 32] to the use of analogies to neutron optics [33, 34]. Throughout this article, we pursue a representation-free approach based on unitary time evolution operators [28, 35–38] and outline our interferometer, evaluate the resulting phase shift and review the present status of the experiment.

### 1.2 At the interface of quantum and gravity

During an impromptu seminar at the NATO Advanced Summer Institute at Bad Windsheim in 1981, Eugene Paul Wigner expressed his discomfort with general relativity [39] in view of quantum mechanics [40]. He emphasized that the notion of a space-time trajectory which is a crucial element of gravity is incompatible with the uncertainty relation of quantum mechanics. Guided by the work of Niels Bohr and Leon Rosenfeld on the limitations of the electromagnetic field [41, 42] due to quantum fluctuations he argued that quantum theory puts severe restrictions on the measurement of the metric tensor representing the gravitational field.

Wigner's thoughts expressed in this seminar were a consequence of his work several decades earlier. Indeed, already in 1958 together with Helmut Salecker he had constructed a clock [43] based on the reflection of light signals from two mirrors and had analyzed the restrictions of the uncertainty relation on the weight of the mirrors.[1]

In this context, it is also worth mentioning that H. Salecker at the *Conference on the Role of Gravitation in Physics* in Chapel Hill in 1957 triggered [45] a discussion on the equivalence principle by a gedanken experiment involving a stream of particles being scattered off a diffraction grating. Greenberger [46] a decade later considered a similar arrangement and even argued that mass in quantum mechanics should be an operator.

The celebrated Colella–Overhauser–Werner (COW) experiment [47] performed in 1975 propelled these and many other thoughts about the interface of quantum and gravity to the real world. Indeed, based on the de Broglie wave nature of neutrons [33] the COW experiment could measure for the first time the phase shift between two arms of a neutron interferometer induced by the gravitational potential of the earth [47–49].

The development of new sources of cold atoms [6] as well as molecules [50], and in particular, the realization of Bose–Einstein condensates [51, 52] has ushered in a new era of experiments to probe quantum mechanics and gravity. Indeed, novel tests of the equivalence principle based on matter-wave interferometry of different isotopes of the same atom [1] such as $^{85}$Rb and $^{87}$Rb or even different species [53] such as $^{39}$K and $^{87}$Rb could be performed. Even the detection of gravitational waves based on atom interferometry is pursued today [54]. Recently, Ref. [55] suggested that gravitational decoherence gives rise to a universal decoherence. Moreover, the atom laser [56] utilizes gravity to form an Airy mode. Furthermore, it is mind-boggling that nowadays measurements of atomic transitions [57, 58] are sensitive to the redshift of the gravitational field.

An extremely interesting development in this realm is again taking place in the field of neutron optics due to the experimental realization of the quantum bouncer [59, 60]. Here neutrons exposed to the gravitational field of the earth are reflected from a surface and oscillate up and down. In particular, they experience a potential consisting of the linear ramp and an infinitely steep wall. It is amazing that a measurement of the transitions between the resulting discrete energy levels can put upper bounds [61] on dark energy and dark matter scenarios.

[1] John Archibald Wheeler frequently emphasized in conversations about this topic and in print [44] that these estimates were too conservative. However, to the best of our knowledge they have never been improved.

### 1.3 Drive for enhanced sensitivity

Hopefully these examples convey the excitement in this field of quantum optics and gravity. Notwithstanding the fact that we still do not have a complete understanding of quantum gravity [62] we have come a long way since the early Salecker–Wigner discussions but many questions remain. Indeed, goals such as gravitational wave detection or a compact gravimeter [63] based on atom optics drive the strive for higher sensitivity of these devices.

The Kasevich–Chu atom interferometer [64, 65] is analogous to the neutron interferometer employed by the COW experiment. The Bragg diffraction of the neutron from three crystal planes of a silicon slab are replaced by Raman diffraction of the atom from three standing light crystals. As a result, the phase shift introduced by the gravitational potential is *quadratic* in the time $2T$ the particle spends in the interferometer.

Needless to say a different scaling of the phase shift, for example with $T^3$, would be desirable. In the present article, we propose such an interferometer and describe our progress towards realizing it.

Our device rests on three principles: (*i*) We take advantage of the cubic dependence of the phase in the propagator in a linear potential. (*ii*) We employ two different internal states of the atom which experience different time-independent accelerations, and (*iii*) we close the interferometer in position *and* velocity by a sequence of four laser pulses.

### 1.4 Outline

Our article is organized as follows. Section 2 serves as a motivation. Here we recall that the propagator of a particle in a linear potential contains a phase which is cubic in time.

In Sect. 3 we introduce our interferometer capable of measuring the cubic phase accumulated by a particle during its motion in a linear potential provided by a constant gravitational field and a magnetic field gradient. The three-level atom probing these fields has two ground states associated with two different magnetic moments and experiences a sequence of four Raman pulses. To close the interferometer in position *and* velocity, we choose the separation of $T - 2T - T$ between the pulses. The resulting probability for the atom to exit the interferometer in one of the two ground states is the familiar oscillatory function. However, in contrast to standard interferometers its argument now depends solely on the phase cubic in $T$ and the discrete third derivative of the laser phase.

We dedicate Sect. 4 to a comparison of our scheme to the Kasevich–Chu interferometer [36, 64–67] and distinguish the cubic phase shift from the ones caused by a gravity gradient or the Continuous-Acceleration Bloch (CAB) technique [12]. In Sect. 5 we discuss a possible experimental implementation of our proposal. We conclude in Sect. 6 by briefly summarizing our results and providing an outlook.

To keep our article self-contained but focused on the central ideas, we include lengthy calculations in five appendices. In Appendix A we show that the Kennard phase depends on the initial wave function. However, we emphasize that in our arrangement the resulting interferometer phase which is cubic in time is independent of the initial state of the center-of-mass motion. In Appendix B we recall the technique of creating coherent superpositions of the two atomic ground states and interchanging their populations using Raman pulses. We then turn in Appendix C to a description of our interferometer as a sequence of unitary operators and derive an expression for the phase of our $T^3$-interferometer. In Appendix D we derive the conditions to close our interferometer and obtain in Appendix E an explicit formula for the resulting phase. It is interesting that this result also follows from the formalism of Refs. [37, 38].

## 2 From global to interferometer phase

The propagator of a quantum particle experiencing a linear potential is determined by a phase factor governed by the corresponding classical action. Since the relevant classical motion involves time in the coordinate and velocity in a quadratic and a linear way, both the kinetic as well as potential energies bring in time quadratically. As a result, the action being the integral over time must contain a term proportional to the cube of time. This cubic phase which is independent of the coordinate is at the center of our interest in the present section.

We first recall the essential features of the propagator for the wave function in a linear potential. Here we focus especially on this cubic phase. Moreover, in Appendix A we show that due to the Huygens principle for matter waves the integration over the initial coordinate leads to a dependence of this phase on the initial wave function.

Although we find this property interesting we emphasize that it is of no importance to the present discussion. Indeed, due to the Born rule we cannot measure the global phase factor of a *single* quantum system. However, an interferometric measurement of the difference of *two* different global phase factors of *two* systems is possible. Especially, for a closed interferometer in which the phase shift does not depend on the initial state also the cubic phase is independent [37, 38] of the initial wave function. We dedicate the second part of this section to this topic.

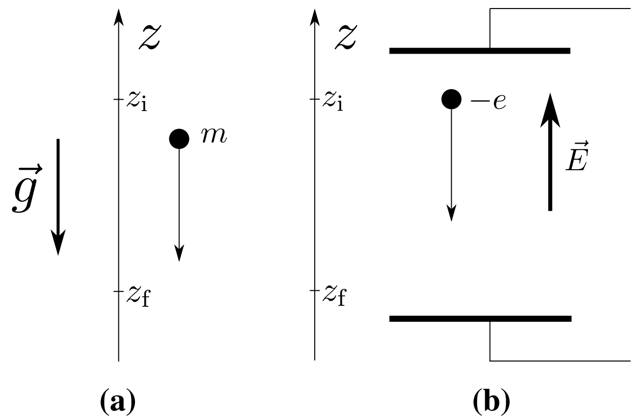


**Fig. 1** Two physical systems with a linear potential $V(z) \equiv -Fz$ corresponding to a constant force $\mathbf{F} = F\mathbf{e}_z$ directed along the $z$-axis: **a** a particle of mass $m$ which experiences the constant gravitational acceleration $g$ with $F \equiv -mg$, and **b** a charge $-e$ in an ideal capacitor with the constant and homogeneous electric field $E$ with $F \equiv -eE$

### 2.1 Emergence of $T^3$-phase in the propagator

We start our analysis by discussing the propagator of a particle in a linear potential. Here we emphasize especially the emergence of the phase factor cubic in time.

We consider a particle of mass $m$ moving in a linear potential $V(z) \equiv -Fz$ corresponding to a constant force $\mathbf{F} \equiv F\mathbf{e}_z$ directed along the $z$-axis with the unit vector $\mathbf{e}_z$. This problem occurs for (1) a particle, which experiences a constant gravitational acceleration $g$ with $F \equiv -mg$ as indicated in Fig. 1a, and (2) a charge $-e$ in an ideal capacitor with the constant electric field $E$, for which $F \equiv -eE$ as shown in Fig. 1b. Throughout this article we focus on the example of a linear gravitational potential.

The wave function

$$\psi(z_\mathrm{f}, t_\mathrm{f}) = \int_{-\infty}^{+\infty} G(z_\mathrm{f}, t_\mathrm{f}|z_\mathrm{i}, t_\mathrm{i})\psi(z_\mathrm{i}, t_\mathrm{i})\mathrm{d}z_\mathrm{i} \tag{1}$$

representing the probability amplitude to find the particle at the final position $z_\mathrm{f}$ at time $t_\mathrm{f}$ is determined by the propagator [2, 3, 8]

$$G(z_\mathrm{f}, t_\mathrm{f}|z_\mathrm{i}, t_\mathrm{i}) \equiv \left\langle z_\mathrm{f} \middle| \exp\left[-\frac{i}{\hbar}\left(\frac{\hat{p}_z^2}{2m} - F\hat{z}\right)(t_\mathrm{f} - t_\mathrm{i})\right] \middle| z_\mathrm{i} \right\rangle, \tag{2}$$

where $\psi(z_\mathrm{i}, t_\mathrm{i})$ is the value of the wave function at the initial position $z_\mathrm{i}$ and time $t_\mathrm{i}$, and $\hat{z}$ and $\hat{p}_z$ denote the position and momentum operators, respectively.

The propagator $G$ defined by Eq. (2) can be cast [8] in terms of the classical action

$$\begin{aligned} S_\mathrm{cl}(z_\mathrm{f}, t_\mathrm{f}|z_\mathrm{i}, t_\mathrm{i}) &\equiv \int_{t_\mathrm{i}}^{t_\mathrm{f}} L\big(z_\mathrm{cl}(t), \dot{z}_\mathrm{cl}(t)\big)\mathrm{d}t \\ &= \frac{m}{2}\frac{(z_\mathrm{f} - z_\mathrm{i})^2}{t_\mathrm{f} - t_\mathrm{i}} + \frac{F}{2}\big(z_\mathrm{f} + z_\mathrm{i}\big)(t_\mathrm{f} - t_\mathrm{i}) - \frac{F^2}{24m}(t_\mathrm{f} - t_\mathrm{i})^3 \end{aligned} \tag{3}$$

along the classical trajectory given by

$$z_\mathrm{cl}(t) \equiv z_\mathrm{i} + \frac{z_\mathrm{f} - z_\mathrm{i}}{t_\mathrm{f} - t_\mathrm{i}}(t - t_\mathrm{i}) + \frac{F}{2m}(t - t_\mathrm{i})(t - t_\mathrm{f}) \tag{4}$$

and

$$\dot{z}_\mathrm{cl}(t) \equiv \frac{d}{dt}z_\mathrm{cl}(t) = \frac{z_\mathrm{f} - z_\mathrm{i}}{t_\mathrm{f} - t_\mathrm{i}} + \frac{F}{m}\left(t - \frac{t_\mathrm{i} + t_\mathrm{f}}{2}\right). \tag{5}$$

Here we have used the Lagrangian

$$L(z, \dot{z}) \equiv \frac{m}{2}\dot{z}^2 + Fz \tag{6}$$

of a particle in a linear potential.

Indeed, the representation

$$G(z_\mathrm{f}, t_\mathrm{f}|z_\mathrm{i}, t_\mathrm{i}) = N(t_\mathrm{f} - t_\mathrm{i}) \exp\left[\frac{i}{\hbar}S_\mathrm{cl}(z_\mathrm{f}, t_\mathrm{f}|z_\mathrm{i}, t_\mathrm{i})\right] \tag{7}$$

with the normalization

$$N(\tau) \equiv \sqrt{\frac{m}{2i\pi\hbar\tau}} \tag{8}$$

brings out most clearly that $G$ contains the phase

$$\phi(\tau) \equiv -\frac{1}{24}\frac{F^2}{\hbar m}\tau^3, \tag{9}$$

which is independent of the initial and final positions $z_\mathrm{i}$ and $z_\mathrm{f}$, and scales with the third power of the time difference

$$\tau \equiv t_\mathrm{f} - t_\mathrm{i}, \tag{10}$$

that is the time during which the particle experiences the constant force $F$.

### 2.2 How to observe the $T^3$-phase?

The propagator $G$ defined in Eq. (7) contains a global phase $\phi$ given by Eq. (9) which is cubic in time, proportional to the square of the constant force $F$, and inversely proportional to the mass $m$ of the particle. However, due to the integration over the initial position in the Huygens integral, Eq. (1), this phase depends, as exemplified in Appendix A, on the initial wave function. We now briefly outline our strategy for measuring this phase and emphasize that for our closed interferometer the resulting phase is independent of the initial state.

Obviously a setup providing us only with the probability density $|\psi(z_\mathrm{f}, t_\mathrm{f})|^2$ is insensitive to any global phase like the $T^3$-phase. Therefore, we need to involve an interferometric

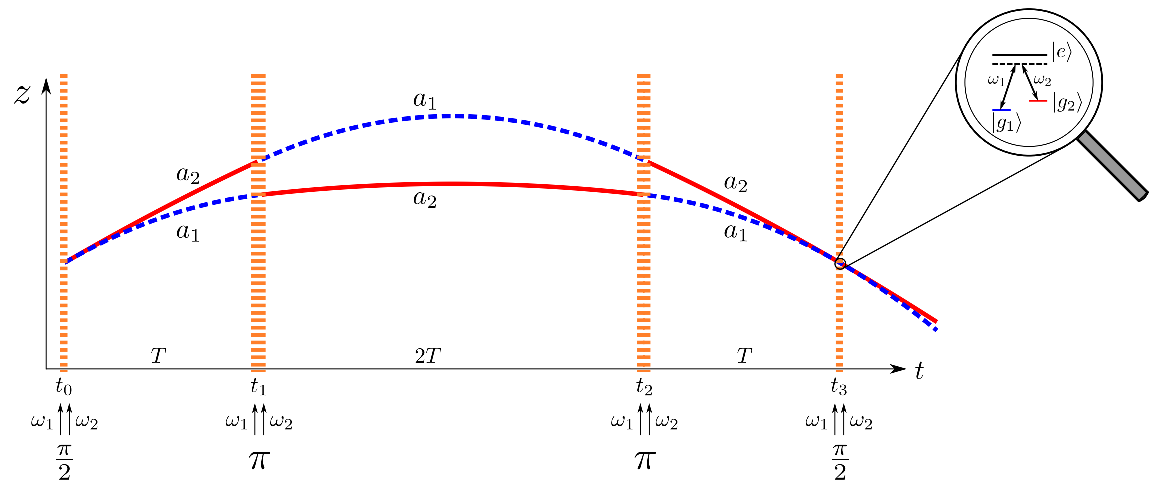


**Fig. 2** Space-time diagram of the $T^3$-interferometer for a three-level atom consisting of the states $|g_1\rangle$, $|g_2\rangle$, and $|e\rangle$, and interacting with four short Raman laser pulses at $t = t_0$, $t = t_1 \equiv t_0 + T$, $t = t_2 \equiv t_0 + 3T$ and $t = t_3 \equiv t_0 + 4T$. The laser frequencies $\omega_1$ and $\omega_2$ are assumed to only drive the transitions $|g_1\rangle \longleftrightarrow |e\rangle$ and $|g_2\rangle \longleftrightarrow |e\rangle$, respectively

measurement either with a path-dependent strength of the constant force, or a path-dependent mass of the particle.

Throughout this article we focus on the first alternative although we can imagine possibilities[2] to utilize the dependence of the mass on the internal state. Key elements of our technique are: (*i*) an atom with two internal states associated with two different magnetic moments, and (*ii*) an external time-independent magnetic field with a constant gradient along one direction. Due to the Zeeman effect, the atom experiences a constant force determined by its internal state. It is the same force that acts on a classical magnetic dipole in a non-uniform magnetic field.

## 3 Atom interferometer with four light pulses

In this section, we introduce the two crucial elements of our $T^3$-interferometer: (*i*) the population dynamics of the two resonant states of the atom driven by the Raman laser pulses, and (*ii*) the Zeeman shift of the atomic levels induced by the external time-independent magnetic field with a constant gradient along one direction. The description of our interferometer is based on the representation-free approach described in Refs. [28, 35, 36].

[2] According to Ref. [68] mass and proper time are conjugate variables and two internal states of the atom correspond [7, 32] to two different masses giving rise to an additional phase shift [54] for the atom prepared in a superposition state. Although this effect is minute the improved scaling of the Kennard phase might help to identify this effect.

### 3.1 Population dynamics

We are now in the position to present our atom interferometer capable of measuring the cubic phase. The general scheme depicted in Fig. 2 consists of two distinct "building blocks": (*i*) four Raman pulses, that is two $\frac{\pi}{2}$- and two $\pi$-pulses, which form a $\frac{\pi}{2} - \pi - \pi - \frac{\pi}{2}$ sequence, and (*ii*) three regions of the atomic center-of-mass motion with constant accelerations $a_1$ and $a_2$.

We consider a three-level atom consisting of the ground state $|g_1\rangle$, the state $|g_2\rangle$, and the excited state $|e\rangle$. Here $|g_1\rangle$ and $|g_2\rangle$ are chosen such that the mean values of their magnetic moment are different, which leads to a state-dependent acceleration and magnetically induced phase shifts [69, 70]. The center-of-mass motion of the atom is assumed to be along the $z$-axis, which is the direction of the constant gravitational acceleration.

Thus, we arrive at the Hamiltonian

$$\begin{aligned}\hat{H}_{\text{at}} \equiv \mathbb{1}_3 \otimes \frac{\hat{p}_z^2}{2m} + |e\rangle\langle e| \otimes \left(E_e \mathbb{1}_z - m a_e \hat{z}\right)\\ + |g_1\rangle\langle g_1| \otimes \left(E_{g_1} \mathbb{1}_z - m a_1 \hat{z}\right)\\ + |g_2\rangle\langle g_2| \otimes \left(E_{g_2} \mathbb{1}_z - m a_2 \hat{z}\right),\end{aligned} \tag{11}$$

of the three-level atom, where

$$\mathbb{1}_3 \equiv |e\rangle\langle e| + |g_1\rangle\langle g_1| + |g_2\rangle\langle g_2|$$

and

$$\mathbb{1}_z \equiv \int_{-\infty}^{+\infty} \mathrm{d}z\, |z\rangle\langle z|$$

are the identity operators corresponding to the Hilbert space of the internal atomic states, and the center-of-mass motion along the $z$-axis, respectively. Here $E_e$, $E_{g_1}$, and $E_{g_2}$ are the energies of the atom in the internal states $|e\rangle$, $|g_1\rangle$, and $|g_2\rangle$, respectively, with $a_e$ being the constant acceleration corresponding to the excited state.

Each block of our $T^3$-interferometer is described in terms of an appropriate unitary operator. As discussed in more detail in Appendix B, the atom–light interaction is accounted for by the evolution operator

$$\hat{U}_{\mathrm{p}}(\theta) \equiv \left( |g_1\rangle\langle g_1| + |g_2\rangle\langle g_2| \right) \cos\left(\frac{\theta}{2}\right) - i\left(e^{i\phi_{\mathrm{L}}}|g_1\rangle\langle g_2| + e^{-i\phi_{\mathrm{L}}}|g_2\rangle\langle g_1|\right) \sin\left(\frac{\theta}{2}\right), \tag{12}$$

where $\phi_{\mathrm{L}}(t) \equiv \phi_2 - \phi_1$ is the difference of the phases $\phi_1$ and $\phi_2$ of the two lasers used for the Raman transition and $\theta$ denotes the total pulse area. Moreover, we have assumed that each Raman pulse consists of two co-propagating laser beams with almost identical wavelengths which makes $\hat{U}_{\mathrm{p}}$ given by Eq. (12) independent of $z$. Hence, there is no momentum transfer from the light to the atom.

On the other hand, the operator

$$\hat{U}_a(t_{\mathrm{f}}, t_{\mathrm{i}}) \equiv \exp\left[-\frac{i}{\hbar}\left(\frac{\hat{p}_z^2}{2m} - ma\hat{z}\right)(t_{\mathrm{f}} - t_{\mathrm{i}})\right] \tag{13}$$

with $a = a_1$ or $a = a_2$ provides us with the center-of-mass motion.

In Appendices C and D we analyze the interferometer of Fig. 2 as a sequence of these unitary operators and find the expression

$$P_{g_2} = \frac{1}{2}\left[1 + \cos\left(\varphi_{\mathrm{i}} + \varphi_{\mathrm{L}}\right)\right] \tag{14}$$

for the probability of observing the atoms in the state $|g_2\rangle$ after the action of the four Raman pulses. According to Appendix E, the interferometer phase $\varphi_{\mathrm{i}}$ reads

$$\varphi_{\mathrm{i}} \equiv \frac{m}{\hbar}(a_1^2 - a_2^2)T^3, \tag{15}$$

and in Appendix C we derive the formula

$$\varphi_{\mathrm{L}} \equiv \phi_{\mathrm{L}}(t_0) - 2\phi_{\mathrm{L}}(t_0 + T) + 2\phi_{\mathrm{L}}(t_0 + 3T) - \phi_{\mathrm{L}}(t_0 + 4T) \tag{16}$$

for the contribution due to the phases $\phi_L$ of the four laser pulses.

We emphasize that this result is independent of the initial state of the center-of-mass motion. This property of the *interferometer phase* is in sharp contrast to the dependence of *global phase* of Appendix A corresponding to a *single* degree of freedom, and is a consequence [28, 37, 38] of the fact that our interferometer is closed in both position *and* velocity.

### 3.2 Zeeman effect: control of external degrees of freedom

Next, we turn to a possible realization of our interferometer scheme, and in particular, of the accelerations $a_1$ and $a_2$. To make contact with the experiment discussed in Sect. 5, we consider a special case.

For this purpose we focus on the interaction of the atom with a time-independent magnetic field having locally the form[3]

$$\mathbf{B}(\mathbf{r}) \cong \left(B_0 + z\,\nabla_z B_z\right)\mathbf{e}_z \tag{17}$$

which results in the linear Zeeman shifts

$$\Delta E_{g_1}^Z = \mu_B g_{F_1} m_{F_1}\left(B_0 + z\,\nabla_z B_z\right) \tag{18}$$

and

$$\Delta E_{g_2}^Z = \mu_B g_{F_2} m_{F_2}\left(B_0 + z\,\nabla_z B_z\right) \tag{19}$$

of the energies of $|g_1\rangle$ and $|g_2\rangle$. Here $\mu_B$, $g_{F_1}$, $g_{F_2}$, $m_{F_1}$, and $m_{F_2}$ denote the Bohr magneton, the Landé $g$-factors of $|g_1\rangle$ and $|g_2\rangle$, and the magnetic quantum numbers associated with the $z$-component of the angular momentum corresponding to $|g_1\rangle$ and $|g_2\rangle$.

The homogeneous magnetic field $B_0$ leads to an energy shift of the magnetive sensitive states and together with the constant gravitational field we arrive at the expressions

$$a_1 \equiv -g - \frac{\mu_B}{m} g_{F_1} m_{F_1} \nabla_z B_z \tag{20}$$

and

$$a_2 \equiv -g - \frac{\mu_B}{m} g_{F_2} m_{F_2} \nabla_z B_z \tag{21}$$

for the accelerations of the atomic center-of-mass corresponding to $|g_1\rangle$ and $|g_2\rangle$, respectively.

In our experiment, we use the D2 transition of $^{85}$Rb and choose $|g_1\rangle$ and $|g_2\rangle$ from the $F = 2$ and $F = 3$ hyperfine state manifolds. For the atomic transition $|F_1 = 2, m_{F_1} = 1\rangle \to |F_2 = 3, m_{F_2} = 1\rangle$ the interferometer phase given by Eq. (15) reduces to

$$\varphi_i = \frac{4}{3}\frac{\mu_B}{\hbar}\nabla_z B_z g T^3\ , \tag{22}$$

[3] Throughout the article, we use the notation $\nabla_z B_z \equiv \frac{\partial B_z}{\partial z}(\mathbf{r} = 0)$ for the derivative of the $z$-component of the magnetic field $\mathbf{B} = \mathbf{B}(\mathbf{r})$ along the $z$-direction at the origin $\mathbf{r} = 0$. This derivative is assumed to be small compared to $B_0$, such that $L|\nabla_z B_z| \ll |B_0|$, where $L$ is the total length of the interferometer. Moreover, we note that the form of the magnetic field given by Eq. (17) is an approximate one. Indeed, according to the Maxwell equation $\nabla \cdot \mathbf{B} = 0$, which is valid everywhere, a non-zero value of $\nabla_z B_z$ induces non-zero values of $\nabla_x B_x$ and $\nabla_y B_y$, such that $\nabla_x B_x + \nabla_y B_y = -\nabla_z B_z$, where $B_x$ and $B_y$ are the components of $\mathbf{B}$ along the $x$- and $y$-axis. However, in the limit of $L|\nabla_z B_z| \ll |B_0|$ the magnetic field $\mathbf{B}$ given by Eq. (17) is approximately directed along the $z$-axis.

where we have used the fact [71] that $g_{F_2} = -g_{F_1} = 1/3$.

## 4 Discussion

In the preceding section, we have derived an expression for the probability of finding the atom in the state $|g_2\rangle$ at one exit of our interferometer. In the present section, we compare and contrast our device with the Kasevich–Chu interferometer, and make contact with other cubic phases such as the ones caused by a gravity gradient, or arising in the CAB technique.

### 4.1 Comparison with Kasevich–Chu interferometer

We first recall the expressions corresponding to Eqs. (14), (15) and (16) and then discuss the similarities and differences between these two devices. A brief analysis of the respective scale factors concludes this comparison.

#### 4.1.1 General considerations

In the Kasevich–Chu interferometer, the probability corresponding to Eq. (14) reads [11, 29, 36, 64, 65, 67]

$$P_{g_2}^{(KC)} = \frac{1}{2}\left[1 - \cos\left(\varphi_{\mathrm{i}}^{(KC)} + \varphi_{\mathrm{L}}^{(KC)}\right)\right] \tag{23}$$

with the interferometer phase

$$\varphi_{\mathrm{i}}^{(KC)} \equiv (k_1 + k_2) g T^2 \tag{24}$$

and the total laser phase

$$\varphi_{\mathrm{L}}^{(KC)} \equiv \phi_{\mathrm{L}}(t_0) - 2\phi_{\mathrm{L}}(t_0 + T) + \phi_{\mathrm{L}}(t_0 + 2T). \tag{25}$$

We note four major differences between our scheme and that of Kasevich–Chu: (*i*) The *four* rather than the *three* Raman pulses create the *sum* of the two terms appearing in the square brackets of $P_{g_2}$ given by Eq. (14) rather than the *difference* in $P_{g_2}^{(KC)}$ defined by Eq. (23). In the absence of any potentials the different pulse sequences correspond to a $2\pi$-rotation on the Bloch sphere in the case of the Kasevich–Chu interferometer, and a $3\pi$-rotation for our $T^3$-interferometer giving rise to the opposite signs. (*ii*) The phase $\varphi_{\mathrm{i}}$ induced by the linear potentials and given by Eq. (15) depends on the separation $T$ of the pulses in a *cubic* rather than *quadratic* way as in $\varphi_{\mathrm{i}}^{(KC)}$ expressed by Eq. (24). (*iii*) *Co-propagating* laser beams together with a constant magnetic field gradient lead to a proportionality of $\varphi_{\mathrm{i}}$ to $\nabla_z B_z$ as reflected by Eq. (22), while in the case of Kasevich–Chu the use of *counter-propagating* laser beams results in a momentum transfer of $\pm\hbar(k_1 + k_2)$ which reflects itself in $\varphi_{\mathrm{i}}^{(KC)}$. (*iv*) The total laser phase $\varphi_{\mathrm{L}}$ defined by Eq. (16) is a discrete *third* derivative rather than the *second* one for $\varphi_{\mathrm{L}}^{(KC)}$ given by Eq. (25). Indeed, this feature becomes obvious when we consider the limit of $T \to 0$, for which $\varphi_{\mathrm{L}} \cong -2\dddot{\varphi}_{\mathrm{L}}(t_0)T^3$ while [36, 67] $\varphi_{\mathrm{L}}^{(KC)} \cong \ddot{\varphi}_{\mathrm{L}}(t_0)T^2$, with $\dddot{\varphi}_{\mathrm{L}}(t_0)$ and $\ddot{\varphi}_{\mathrm{L}}(t_0)$ being the third and second continuous derivatives of the phase $\varphi_{\mathrm{L}} = \varphi_{\mathrm{L}}(t)$ of the Raman pulse, respectively.

#### 4.1.2 Scale factors and limitations

Next, we turn to a comparison between the scale factors of the two interferometers. We first note that the phases $\varphi_i$, Eq. (22), and $\varphi_i^{(KC)}$, Eq. (24), are both (*i*) linear proportional to the gravitational acceleration $g$, (*ii*) independent of the atomic mass $m$, and (*iii*) determined only by classical quantities, that is Eqs. (22) and (24) do not include the Planck constant $\hbar$. For the latter statement we keep in mind that the Bohr magneton $\mu_B$ is linearly dependent on $\hbar$.

However, we emphasize that the difference in the scale factors due to the appearance of the gradient of the magnetic field in the phase $\varphi_i$, Eq. (22), rather than the sum of the wave vectors in $\varphi_i^{(KC)}$, Eq. (24), is crucial for the scale factor stability. Indeed, in our experiment discussed in more detail in Sect. 5 we have found that the stability of the magnetic field as measured by the frequency difference of the two transitions $|F_1 = 2, m_{F_1} = 0\rangle \to |F_2 = 3, m_{F_2} = 0\rangle$ and $|F_1 = 2, m_{F_1} = 0\rangle \to |F_2 = 3, m_{F_2} = 1\rangle$ did not vary more than 0.1 % without sophisticated electronic feedback or magnetic shielding. In contrast, the scale factor stability of the Kasevich–Chu interferometer can be estimated to be 1 part in $10^{10}$ due to the use of the wave vector of the light. Hence, in this respect the Kasevich–Chu interferometer is superior compared to our device.

Although our interferometer scales with $T^3$ rather than with $T^2$ as the Kasevich–Chu interferometer, $\varphi_i$ is larger than $\varphi_i^{(KC)}$ only for $T >$ 0.23 s with $\nabla_z B_z = 600\,\mu\mathrm{T/m}$ and $k_1 + k_2 \approx 1.6 \times 10^7\,\mathrm{m}^{-1}$ [72]. Moreover, it is important to note that nowadays a beamsplitter with large momentum transfer [73, 74] allows to increase $\varphi_i^{(KC)}$ by a few orders of magnitudes.

In the presence of a magnetic field gradient $\nabla_z B_z = 600\,\mu\mathrm{T/m}$ as measured in our experiment, we have one complete oscillation of the excited state population $P_{g_2}$, Eq. (14), for $T \gtrsim 2.1$ ms. However, if the signal-to-noise ratio allows it one could see the different dependence on $T$ even for short times as demonstrated in Ref. [12].

### 4.2 Other origins of cubic phases

We now compare and contrast the $T^3$-phase in our interferometer induced by the propagator of a particle in a linear potential to other phases cubic in time. Here we focus on two different situations: (*i*) the presence of a gravity gradient, or (*ii*) the application of the CAB technique.

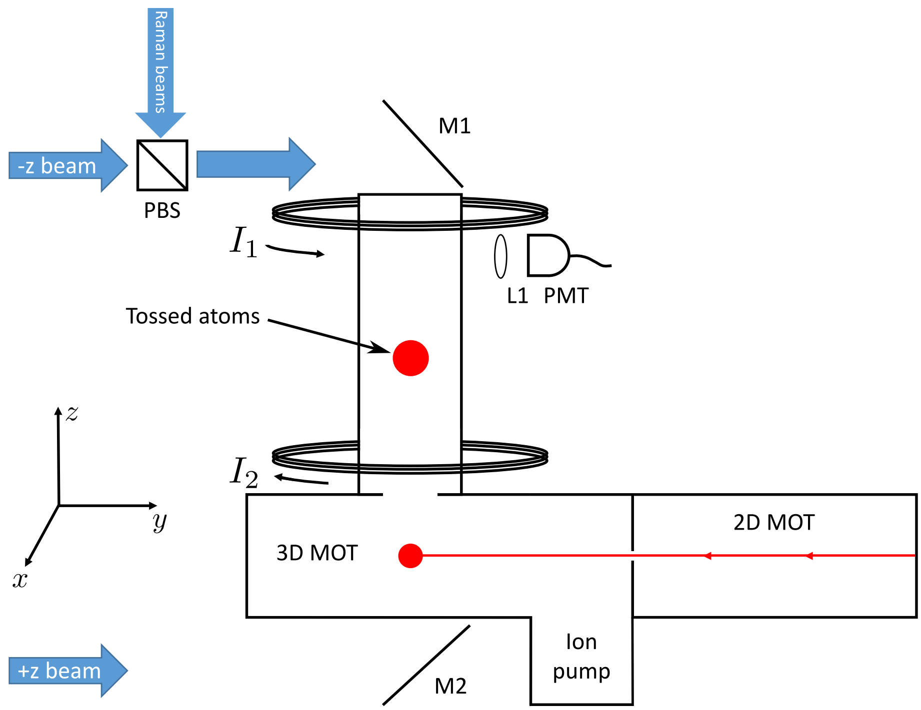


**Fig. 3** Experimental setup for the $T^3$-interferometer. Our $^{85}$Rb atoms emerge from a two-dimensional magneto-optical trap (2D MOT), pass through an aperture into the 3D MOT as indicated by the *red line*, and are then launched into a glass tower in a moving molasses configuration. The mirrors $M_1$ and $M_2$ reflect the $+z$ and $-z$ beams of the 3D MOT, respectively, as well as the two co-propagating Raman beams with the parallel circular polarizations, used for the control of the internal atomic states. We employ two coils in an anti-Helmholtz configuration with currents $I_1$ and $I_2$ to create a magnetic field with constant gradient in the $z$-direction along the glass tower. A solenoid not depicted here surrounds the tower to provide an additional nominally uniform magnetic field. The lens $L_1$ collects the fluorescence from the tossed atoms at the top of the tower and focuses this light onto a photomultiplier (PMT)

#### *4.2.1 Gravity gradient*

In the presence of a gravity gradient $\Gamma$ a phase cubic in time appears [28–31, 37] in the Kasevich–Chu interferometer as a consequence of a *single quadratic* potential

$$V_\Gamma(z) \equiv mgz + \frac{1}{2}m\Gamma z^2 \tag{26}$$

rather than *two linear* potentials. In particular, it results from an expansion of the atomic center-of-mass motion in the limit of a weak gravity gradient, that is $\Gamma T^2 \ll 1$. Indeed, a gravity gradient leads to a *position-dependent* acceleration, while the two linear potentials in our interferometer lead to a *state-dependent* acceleration.

Furthermore, we emphasize that the Kasevich–Chu interferometer is no longer closed in position *and* velocity in the presence of a gravity gradient. This deficiency leads to a loss of contrast [37] and a dependence of the phase shift on the initial state.

The interferometer can be closed (at least approximately) by additional laser pulses [17] or by suitably adjusting the laser wavelength of the intermediate pulse [75]. However, this procedure also eliminates the cubic contributions to the phase shift, in contrast to the situation considered here.

#### *4.2.2 Continuous-acceleration-Bloch technique*

Our $T^3$-interferometer shares the underlying idea of CAB [12, 13], that is applying different accelerations along each interferometer arm. However, instead of achieving these accelerations via state-dependent linear potentials, a beam splitter based on Bragg diffraction is used to load one of the two exit ports into an optical lattice, which is accelerated subsequently by the use of Bloch oscillations.

While in our scheme we can close the interferometer easily in position *and* velocity by simply choosing the correct timing between the pulses, the CAB scheme requires a sophisticated control of the time-dependent acceleration of the optical lattice. Moreover, we emphasize that in contrast to the $T^3$-interferometer, in the CAB scheme not only a phase proportional to $T^3$, but also one proportional to $T^2$ emerges.

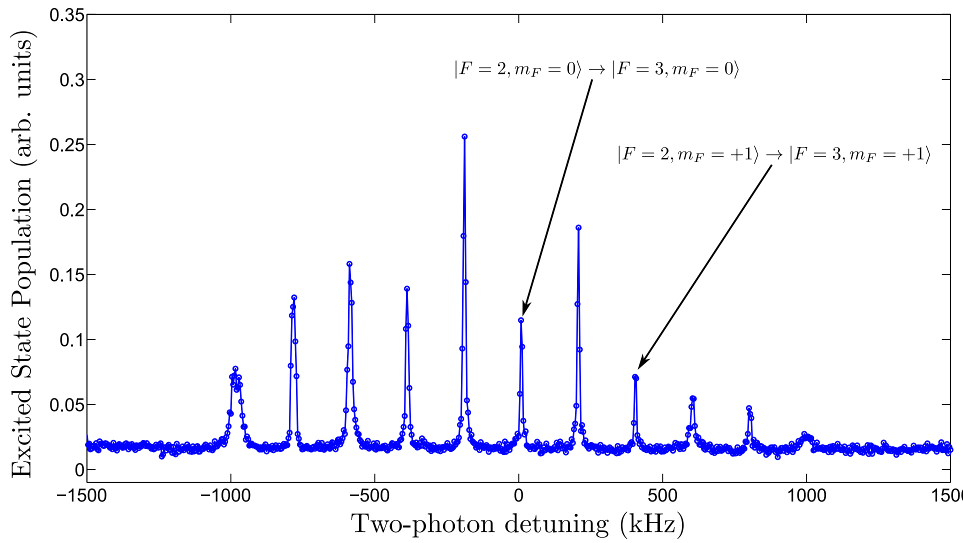


**Fig. 4** Typical Raman spectrum containing the transitions between the states of the $F = 2$ and $F = 3$ manifolds for an arbitrarily aligned magnetic field in their dependence on the two-photon detuning $\tilde{\Delta}$ defined by Eq. (27) with respect to the clock transition, for which resonance occurs at $\tilde{\Delta} = 0$. We observe 11 resonances corresponding to 5 or 6 transitions with $\Delta m_F = 0$ or $\Delta m_F = \pm 1$, respectively. Transitions with $\Delta m_F = \pm 2$ are heavily suppressed [76, 77]

## 5 Towards an experimental realization

In this section, we discuss a possible experimental implementation of our proposal for a $T^3$-interferometer based on our current laboratory apparatus depicted in Fig. 3. We first summarize the key features of our setup, describe our method to deduce the magnetic fields from the observed Raman spectra, and conclude by briefly analyzing the present limitation of our device due to decoherence.

### 5.1 Experimental setup

We use the D2 transition of $^{85}$Rb and choose $|g_1\rangle$ and $|g_2\rangle$ from the $F = 2$ and $F = 3$ hyperfine state manifolds with a frequency separation of approximately 3 GHz [76]. The atoms are loaded into a three-dimensional magneto-optical trap (3D MOT) emerging from a two-dimensional trap (2D MOT) as shown in Fig. 3. The 3D MOT consists of standard cooling and repump beams as well as magnetic coils. We rely on an all-glass chamber as our vacuum system.

After 1 s of loading to obtain a sufficient signal-to-noise ratio, the atoms are launched upwards along the $z$-axis in a moving optical molasses configuration with a velocity of approximately 3 m/s such that they strike the top of a 10 cm tall glass tower. It takes the atoms between 20 and 40 ms to reach this point depending on the launch velocity which can be adjusted by the voltage of the launch signal. We emphasize that the top of the tower does not coincide with the apex of the trajectory.

After launch, the atoms are freely moving in the dark and we are able to apply a single or several Raman pulses involving two co-propagating laser beams along the $z$-axis with the same circular polarization. During their motion the atoms interact with a magnetic field which varies linearly along the $z$-axis due to coils in an anti-Helmholtz configuration which are not the ones used to trap the atoms. Moreover, they feel the field of a solenoid of finite length not depicted in Fig. 3 surrounding the glass tower. The ability to change the current independently in each of the gradient coils and the solenoid provides us with the control of the location of the zero crossing of the magnetic field, or an effective way to adjust the bias field.

On the top of the tower a photomultiplier tube (PMT) detector performs a projective measurement of the population in the state $|g_2\rangle$ by collecting the fluorescence emitted by the atoms caused by the vertical trapping beams, that is the $+z$ and $-z$ beams, which are switched back on for the measurement. Observing the atomic population always at the top of the tower provides us with a convenient way of varying the position where the Raman pulse is applied to the atoms along their flight path.

### 5.2 Raman spectrum

With this setup we can map out the magnetic field along the atom trajectory by measuring Raman spectra of the type shown in Fig. 4. For this purpose we first use an optical pumping stage to transfer all atoms to the ground state $|g_1\rangle$, that is the state with $F = 2$. Then we apply a Raman light pulse whose intensity and duration are chosen to be close to a zero-detuning $\pi$-pulse. We have found that this condition is satisfied for a pulse duration of 25–100 μs, using our typical total Raman power of approximately 80 mW in a beam of diameter 2.5 cm and a single photon detuning of 1–2 GHz. Finally, we observe the number of atoms transferred from $|g_1\rangle$ to $|g_2\rangle$, that is the state with $F = 3$.

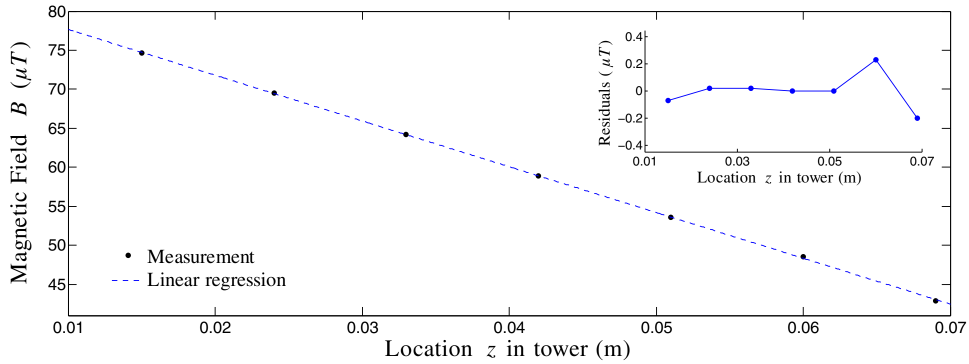


**Fig. 5** Measurement of the magnetic field gradient along the vertical direction in the glass tower. A linear regression of our data points deduced from the Raman spectra with the help of Eq. (29) yields the magnetic field $B(z) = (83.5–587\ \mathrm{m}^{-1}\ z)\ \mu\mathrm{T}$ along the tower and corresponds to a magnetic field gradient of approximately 600 μT/m. The inset shows the residuals of the linear fit. For this measurement we have used the frequency difference between the clock and the +2 transition induced by the Zeeman effect. The magnetic field is generated by currents of 90 mA for the gradient coils and 40 mA for the solenoid

In this manner, we obtain Raman spectra such as the one presented in Fig. 4, that is the population of $|g_2\rangle$ versus the two-photon detuning

$$\tilde{\Delta} \equiv \frac{E_{3,0} - E_{2,0}}{\hbar} + \omega_2 - \omega_1 \tag{27}$$

of the Raman pulse of the frequencies $\omega_1$ and $\omega_2$ with respect to the “clock” transition $|F_1 = 2, m_{F_1} = 0\rangle \to |F_2 = 3, m_{F_2} = 0\rangle$, for which the resonance occurs at $\tilde{\Delta} = 0$. Here $E_{F,m_F}$ denotes the energy of the hyperfine state.

For a magnetic field pointing in an arbitrary direction, the observed Raman spectrum displays up to 11 peaks, that is 5 peaks for $\Delta m_F = 0$ transitions and 6 peaks for $\Delta m_F = \pm 1$ transitions, where $\Delta m_F \equiv m_{F,2} - m_{F,1}$ is the change of the magnetic quantum number. For a magnetic field directed along the $z$-axis as required for the $T^3$-experiment, transitions with $\Delta m_F = \pm 1$ are suppressed in our experimental setup [76, 77].

### 5.3 Magnetic field measurement

The position of the relative two-photon resonance in the Raman spectrum corresponding to the magnetically sensitive transition $|F_1, m_{F_1}\rangle \to |F_2, m_{F_2}\rangle$ is determined by the first-order Zeeman shift

$$\tilde{\Delta}_{F_1,m_{F_1}}^{F_2,m_{F_2}} \equiv \frac{\mu_B}{2\pi\hbar}\left(g_{F_2} m_{F_2} - g_{F_1} m_{F_1}\right) B(z) \tag{28}$$

in frequency, where $B(z)$ is the value of the magnetic field at the center-of-mass coordinate $z$ of the atom cloud during the interaction with the Raman pulse.

Using the +2 transition, that is $|F_1 = 2, m_{F_1} = 1\rangle \to |F_2 = 3, m_{F_2} = 1\rangle$, as indicated in Fig. 4, we determine from the Zeeman shift, Eq. (28), the magnetic field[4]

$$B(z) = 0.11\tilde{\Delta}_{2,1}^{3,1}\,\frac{\mu\mathrm{T}}{\mathrm{kHz}}, \tag{29}$$

where we have used the fact [71] that $m_{F_2} = m_{F_1} = 1$ and $g_{F_2} = -g_{F_1} = 1/3$. It is the opposite signs of $g_{F_2}$ and $g_{F_1}$ that result in the non-degenerate spectrum.

By measuring the resonance frequencies corresponding to the clock and first (or second) peak in the Raman spectrum, we automatically correct for any possible drift in the AC Stark shift caused by a drift in the intensity or frequency of the Raman fields.

We map out the magnetic field experienced by the atoms as a function of their location within the tower, by repeated launching them and applying a Raman pulse at different times after their launch. The corresponding location $z$ of the atom cloud is determined beforehand by time-of-flight photography.

Figure 5 presents the measured magnetic field with a gradient of approximately 600 μT/m generated by a current of 90 mA in the gradient coils and 40 mA in the solenoid.

### 5.4 Imperfect pulses and decoherence

Our proposal for a $T^3$-interferometer presented in the preceding sections assumes that the Raman pulses applied to the atoms are perfect $\frac{\pi}{2}$- and $\pi$-pulses. By definition, such pulses can occur only when the Raman fields are in a two-photon resonance. Since this resonance shifts as the atoms travel up the tower, a rapid detuning of the relative

[4] Only relative positions and magnitudes of the different peaks in the Raman spectrum allow us to determine the different components of the magnetic field [76].

frequency of the Raman fields is necessary. Fortunately, we have been able to achieve this task using a combination of a high-frequency acousto-optic modulator and digital frequency synthesizer, thereby keeping the atoms in resonance during their flight [78].

Unfortunately, a more severe restriction is decoherence and at the moment we identify three culprits: (*i*) magnetic field noise, (*ii*) a non-linear dependence of the magnetic field on $z$, and (*iii*) non-zero components of the magnetic field along the $x$- and $y$-axis.

The upper bound of the magnetic field noise in our setup has been observed to be 50 nT leading to a noise in the magnetic field gradient of about 1 μT/m. The non-linear terms in the dependence of the magnetic field on $z$ lead to an open geometry of our $T^3$-interferometer, and therefore to a loss of contrast [37].

Enforced by the Maxwell equations, the non-zero components of the magnetic field in the $x$- and $y$-direction result in (*i*) a three-dimensional rather than a one-dimensional center-of-mass motion of the atom, and (*ii*) incoherent dynamics of the atomic states involved.

We are currently working on finding an optimal arrangement for the magnetic field and perform numerical simulations of our $T^3$-interferometer.

## 6 Summary and outlook

In the present article, we have proposed an atom interferometer that is sensitive to the quantum mechanical $T^3$-phase emerging in the propagator of a particle in a linear potential. For this purpose we have considered an atom with two magnetic sensitive internal states being exposed to a constant gravitational field as well as a magnetic field with a constant gradient. By applying a sequence of four co-propagating Raman pulses, the atom interferometer can be closed in position *and* velocity. The resulting interferometer phase $\varphi_{\mathrm{i}}$ displays the cubic scaling in $T$ but also depends on the gravitational acceleration and the magnetic field gradient.

We have compared and contrasted this cubic term to the one appearing in the phase of the Kasevich–Chu interferometer in the presence of a gravity gradient, and to the one obtained using the CAB technique. Furthermore, we have outlined a possible experimental realization of our interferometer.

Cubic phases appear frequently in quantum physics and give rise to mind-boggling effects. For example, the energy wave function of a linear potential is given by the Airy function [79] whose standard integral representation involves a cubic phase. This term emerges from the eigenvalue equation in momentum space due to the integration of the kinetic energy which is quadratic in the momentum.

When we suddenly turn-off the potential the so-created Airy wave packet accelerates and its probability density keeps its shape [80] during the free propagation. Deeper insight [66] into this surprising phenomenon springs from Wigner phase space [81] and the fact that the Wigner function of the Airy wave packet is again an Airy function.

Closely related to the cubic phase in the Airy integral and the dispersionless free propagation of the Airy wave packet is the oscillatory probability density created by a point source [9] located in a linear potential and continuously emitting particles into all three space directions with an identical speed. These oscillations appearing in the plane orthogonal to the gravitational force are a consequence of the interference between two classical trajectories of different inclinations. The knowledge of the two distinct paths encoded in the different arrival times is erased by the continuous stream of particles. Again the origin of this particular interference pattern can be traced back to the cubic phase in the Green's function.

Due to the analogy between the constant gravitational field and the constant electric field between two plates of a capacitor discussed in the beginning of this article one might wonder if it is possible to construct a similar charged particle fountain. Indeed, in the case of electrons in a uniform electric field such type of fountain has already been realized in photoionization and photodetachment microscopes [82–84].

It would be fascinating to illuminate the similarities and differences between these three examples of cubic phases and our $T^3$-interferometer. Unfortunately, this task goes beyond the scope of the present article and has to be postponed to future publications.

**Acknowledgements** We are grateful to E. Giese, M. A. Kasevich, S. Kleinert, H. Müller, G. Welch, and W. Zeller for many fruitful discussions on this topic. Moreover, we thank N. Ashby for pointing out Ref. [2] to us. This work is supported by DIP, the German-Israeli Project Cooperation, as well as the German Space Agency (DLR) with funds provided by the Federal Ministry for Economic Affairs and Energy (BMWi) due to an enactment of the German Bundestag under Grants No. DLR 50WM1152-1157 (QUANTUS-IV) and the Centre for Quantum Engineering and Space-Time Research (QUEST). We appreciate the funding by the German Research Foundation (DFG) in the framework of the SFB/TRR-21. W.P.S. is grateful to Texas A&M University for a Texas A&M University Institute for Advanced Study (TIAS) Faculty Fellowship. S.A.D., J.P.D., A.S., and F.A.N. gratefully acknowledge funding from the Office of Naval Research and a grant from the Naval Air Systems Command Chief Technology Office.

## Appendix A: Dependence of $T^3$-phase on initial wave function

According to Sect. 2.1 the cubic phase $\phi$ in the propagator of a quantum particle moving in a linear potential manifests itself in every wave function exposed to this situation. Indeed, since $\phi$ is independent of the initial coordinate $z_\mathrm{i}$ it can be factored out of the Huygens integral for matter waves, Eq. (1).

Nevertheless, the integration of the remaining parts of the propagator in combination with the initial wave function can change the dependence of the phase of the final wave function on the propagation time $\tau = t_f - t_i$. To bring out this fact most clearly we consider the normalized initial wave function

$$\psi(z_\mathrm{i}, t_\mathrm{i}) \equiv \frac{1}{\left(\sqrt{\pi}\Delta z_0\right)^{1/2}} \exp\left(-\frac{z_\mathrm{i}^2}{2\Delta z_0^2}\right) \tag{30}$$

in the form of a real-valued Gaussian of width $\Delta z_0$ and note that wave functions of this kind can be easily realized nowadays in an experiment with cold atoms in a harmonic potential trap.

When we substitute this expression into the Huygens integral of matter waves, Eq. (1), and use the expressions, Eqs. (3) and (7), for the propagator we arrive at the final wave function

$$\psi(z_\mathrm{f}, t_\mathrm{f}) = \frac{1}{\left[\sqrt{\pi}\Delta z(\tau)\right]^{1/2}} \exp\left\{-\frac{\left(z_\mathrm{f} - \frac{F}{2m}\tau^2\right)^2}{2[\Delta z(\tau)]^2} + i\beta\right\} \tag{31}$$

with the time-dependent width

$$\Delta z(\tau) \equiv \Delta z_0 \sqrt{1 + \frac{\tau^2}{\tau_\mathrm{s}^2}} \tag{32}$$

and phase

$$\beta(\tau) \equiv \frac{F z_\mathrm{f} \tau}{\hbar} + \frac{\tau}{\tau_\mathrm{s}} \frac{\left(z_\mathrm{f} - \frac{F}{2m}\tau^2\right)^2}{2[\Delta z(\tau)]^2} - \frac{F^2 \tau^3}{6\hbar m} - \frac{1}{2}\arctan\left(\frac{\tau}{\tau_\mathrm{s}}\right). \tag{33}$$

Here

$$\tau_\mathrm{s} \equiv \frac{m\Delta z_0^2}{\hbar} \tag{34}$$

denotes the spreading time of the wave packet.

We combine the terms in Eq. (33), which are determined by the strength $F$ of the force and independent of the final position $z_\mathrm{f}$, and find the total phase

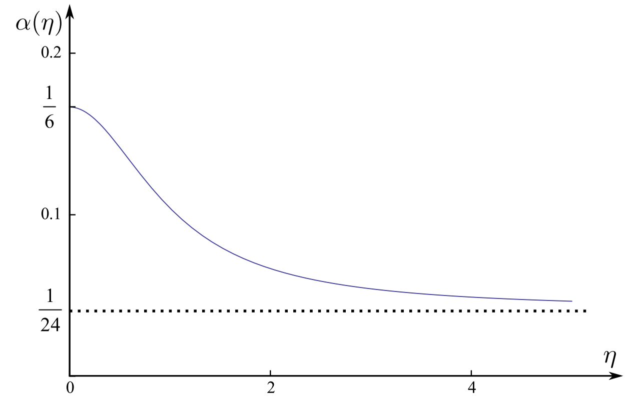


**Fig. 6** Dependence of the numerical factor $\alpha = \alpha(\eta)$ defined by Eq. (36) on the dimensionless ratio $\eta$ of the time difference $\tau$ and spreading time $\tau_s$ given by Eqs. (10) and (34), respectively. For $\eta \to 0$ and $\eta \to \infty$ the factor $\alpha$ is almost constant and given by 1 / 6 and 1 / 24 (*dashed line*), respectively. However, for values of $\eta$ between these extremes $\alpha$ changes rapidly and thus in this transition domain the phase $\tilde{\phi} = \tilde{\phi}(\tau)$, Eq. (35), is not strictly cubic.

$$\tilde{\phi}(\tau) \equiv -\alpha\left(\frac{\tau}{\tau_s}\right)\frac{F^2}{\hbar m}\tau^3. \tag{35}$$

Here we have introduced the time-dependent numerical factor

$$\alpha(\eta) \equiv \frac{1}{24}\frac{\eta^2 + 4}{\eta^2 + 1} \tag{36}$$

depending on the dimensionless ratio $\eta$ of time difference $\tau$, Eq. (10), and spreading time $\tau_s$, which according to Eq. (34) is proportional to square of the initial width $\Delta z_0$.

For a plane wave we find $\Delta z_0 \to \infty$, and thus $\tau_s \to \infty$ leading us to

$$\alpha(\eta \to 0) = \frac{1}{6}. \tag{37}$$

However, for an infinitely narrow Gaussian with $\Delta z_0 \to 0$, and thus $\tau_s \to 0$, we obtain

$$\alpha(\eta \to \infty) = \frac{1}{24}. \tag{38}$$

So far we have restricted ourselves to the extreme limits of $\eta$. Only in the domains where $\alpha$ is approximately constant do we find a pure cubic phase dependence on $\tau$. Indeed, between the extremes the time dependence is more complicated as expressed in Fig. 6.

## Appendix B: Raman pulses: superpositions and exchanges

In this Appendix, we describe the population dynamics [36, 64, 65] of the two resonant atomic states driven by the

Raman laser pulses. For this purpose we consider the interaction between a three-level atom and two laser pulses of the form

$$\mathbf{E}_1(z,t) \equiv \mathcal{E}_1(t)\cos\left(k_1 z - \omega_1 t + \phi_1\right)$$

and

$$\mathbf{E}_2(z,t) \equiv \mathcal{E}_2(t)\cos\left(k_2 z - \omega_2 t + \phi_2\right), \tag{39}$$

where $\mathcal{E}_j$, $k_j$, $\omega_j$, and $\phi_j$ with $j = 1, 2$ denote the time-dependent envelope, frequency, wave vector, and phase of the $j$th field, respectively.

The laser frequencies $\omega_1$ and $\omega_2$ are assumed to only drive the transitions $|g_1\rangle \longleftrightarrow |e\rangle$ and $|g_2\rangle \longleftrightarrow |e\rangle$, respectively. Moreover, we assume that the laser pulses are so short that the atom does not move significantly during the interaction. Therefore, the position of the center-of-mass of the atom is considered to be fixed during the laser pulses.

Within the rotating-wave approximation [81] and in the limit of far-detuned laser pulses with identical detunings, that is when the Rabi frequencies $\Omega_j(t) \equiv \mathbf{d}_{g_j e} \cdot \mathcal{E}_j(t)/\hbar$ of the transitions $|g_j\rangle \longleftrightarrow |e\rangle$ are much smaller than the detuning $\Delta_j \equiv \omega_j - \omega_{eg_j}$ of the two laser pulses, $|\Delta_j| \gg |\Omega_j|$, and $\Delta \equiv \Delta_1 = \Delta_2$, we can eliminate the excited state $|e\rangle$ and neglect the Stark shifts $|\Omega_j(t)|^2/(4\Delta)$. The resulting effective Hamiltonian [36]

$$\begin{aligned}\hat{H}_{\mathrm{p}} = \hbar\frac{\Omega_1(t)\Omega_2(t)}{4\Delta}\big(&e^{i[\Delta k z + \phi_{\mathrm{L}}]}|g_1\rangle\langle g_2| \\ &+ e^{-i[\Delta k z + \phi_{\mathrm{L}}]}|g_2\rangle\langle g_1|\big)\end{aligned} \tag{40}$$

describes the transitions between the states $|g_1\rangle$ and $|g_2\rangle$ due to the Raman pulses. Here $\mathbf{d}_{g_j e} \equiv \langle g_j|\mathbf{d}|e\rangle$ and $\omega_{eg_j} \equiv (E_e - E_{g_j})/\hbar$ are the dipole moment matrix element and the frequency of the transition $|g_j\rangle \longleftrightarrow |e\rangle$, respectively, with $\Delta k \equiv k_2 - k_1$ and the slowly varying laser phase $\phi_{\mathrm{L}}(t) \equiv \phi_2 - \phi_1$.

To avoid a momentum transfer during the Raman transitions, we assume that the laser pulses propagate in the same directions along the $z$-axis, Eq. (39), and that the difference $\Delta k$ of the two wave vectors is small compared to the size $\delta z$ of the atomic wave packet, that is $|\Delta k|\delta z \ll 1$. In this case the dependence on $z$ in Eq. (40) can be neglected and we arrive at

$$\hat{H}_{\mathrm{p}} \cong \hbar\frac{\Omega_1(t)\Omega_2(t)}{4\Delta}\left(e^{i\phi_{\mathrm{L}}}|g_1\rangle\langle g_2| + e^{-i\phi_{\mathrm{L}}}|g_2\rangle\langle g_1|\right). \tag{41}$$

The interaction of the atom with the two far-detuned Raman pulses, corresponding to Eq. (39), during the time interval $t_{\mathrm{i}} < t < t_{\mathrm{f}}$, and with $\Omega_j(t_{\mathrm{i}}) = \Omega_j(t_{\mathrm{f}}) = 0$, is given by the evolution operator [36]

$$\begin{aligned}\hat{U}_{\mathrm{p}} \equiv 1 &+ \left(-\frac{i}{\hbar}\right)\int_{t_{\mathrm{i}}}^{t_{\mathrm{f}}} \mathrm{d}t\hat{H}_{\mathrm{p}}(t) \\ &+ \left(-\frac{i}{\hbar}\right)^2\int_{t_{\mathrm{i}}}^{t_{\mathrm{f}}} \mathrm{d}t \int_{t_{\mathrm{i}}}^{t} \mathrm{d}t'\hat{H}_{\mathrm{p}}(t)\hat{H}_{\mathrm{p}}(t') + \dots\ ,\end{aligned} \tag{42}$$

which can be expressed as

$$\begin{aligned}\hat{U}_{\mathrm{p}}(\theta) = &\left(|g_1\rangle\langle g_1| + |g_2\rangle\langle g_2|\right)\cos\left(\frac{\theta}{2}\right) \\ &- i\left(e^{i\phi_{\mathrm{L}}}|g_1\rangle\langle g_2| + e^{-i\phi_{\mathrm{L}}}|g_2\rangle\langle g_1|\right)\sin\left(\frac{\theta}{2}\right),\end{aligned} \tag{43}$$

where

$$\theta \equiv \frac{1}{2\Delta}\int_{t_{\mathrm{i}}}^{t_{\mathrm{f}}} \mathrm{d}t\,\Omega_1(t)\Omega_2(t) \tag{44}$$

denotes the total pulse area.

The case $\theta = \frac{\pi}{2}$, which is a $\frac{\pi}{2}$-pulse, gives rise [67] to the coherent superpositions

$$\hat{U}_{\mathrm{p}}\left(\frac{\pi}{4}\right)|g_1\rangle = \frac{1}{\sqrt{2}}\left(|g_1\rangle - ie^{-i\phi_{\mathrm{L}}}|g_2\rangle\right)$$

and

$$\hat{U}_{\mathrm{p}}\left(\frac{\pi}{4}\right)|g_2\rangle = \frac{1}{\sqrt{2}}\left(|g_2\rangle - ie^{i\phi_{\mathrm{L}}}|g_1\rangle\right). \tag{45}$$

In contrast, the case $\theta = \pi$, known as a $\pi$-pulse describes an exchange

$$\hat{U}_{\mathrm{p}}\left(\frac{\pi}{2}\right)|g_1\rangle = -ie^{-i\phi_{\mathrm{L}}}|g_2\rangle$$

and

$$\hat{U}_{\mathrm{p}}\left(\frac{\pi}{2}\right)|g_2\rangle = -ie^{i\phi_{\mathrm{L}}}|g_1\rangle \tag{46}$$

of the level populations.

## Appendix C: Interferometer: sequence of unitary operators

Unitary operators describe both the interaction of the atom with the four Raman pulses and the time evolution associated with the center-of-mass motion. In the present Appendix, we derive the complete quantum state of the atom consisting of the internal states as well as the center-of-mass in the two exit ports of our interferometer following the procedure outlined in Refs. [28, 36, 67].

The dynamics in our interferometer consists of the following steps:

1. Before the first $\frac{\pi}{2}$-pulse, at $t = t_0 - \varepsilon$, the initial state
$$|\Psi(t_0 - \varepsilon)\rangle \equiv |g_1\rangle|\psi_0\rangle \tag{47}$$
consists of the center-of-mass motion $|\psi_0\rangle$ and the internal state $|g_1\rangle$. Here and throughout this Appendix $\varepsilon$ is an infinitesimally small and positive number.
2. After the first $\frac{\pi}{2}$-pulse at $t = t_0 + \varepsilon$, the state reads
$$\begin{aligned}|\Psi(t_0 + \varepsilon)\rangle &= \hat{U}_\mathrm{p}\left(\frac{\pi}{4}\right)|\Psi(t_0 - \varepsilon)\rangle \\ &= \left(\frac{1}{\sqrt{2}}|g_1\rangle - \frac{i}{\sqrt{2}}e^{-i\phi_\mathrm{L}(t_0)}|g_2\rangle\right)|\psi_0\rangle,\end{aligned} \tag{48}$$
where we have used Eq. (45).
3. Before the first $\pi$-pulse at $t = t_1 - \varepsilon$, we find
$$\begin{aligned}|\Psi(t_1 - \varepsilon)\rangle &= \hat{U}_a\big(t_1, t_0\big)|\Psi(t_0 + \varepsilon)\rangle \\ &= \frac{1}{\sqrt{2}}|g_1\rangle\hat{U}_{a_1}(t_1, t_0)|\psi_0\rangle \\ &\quad - \frac{i}{\sqrt{2}}e^{-i\phi_\mathrm{L}(t_0)}|g_2\rangle\hat{U}_{a_2}(t_1, t_0)|\psi_0\rangle.\end{aligned} \tag{49}$$
4. After the first $\pi$-pulse at $t = t_1 + \varepsilon$, we obtain
$$\begin{aligned}|\Psi(t_1 + \varepsilon)\rangle &= \hat{U}_\mathrm{p}\left(\frac{\pi}{2}\right)|\Psi(t_1 - \varepsilon)\rangle \\ &= -\frac{i}{\sqrt{2}}e^{-i\phi_\mathrm{L}(t_1)}|g_2\rangle\hat{U}_{a_1}(t_1, t_0)|\psi_0\rangle \\ &\quad - \frac{1}{\sqrt{2}}e^{-i[\phi_\mathrm{L}(t_0)-\phi_\mathrm{L}(t_1)]}|g_1\rangle\hat{U}_{a_2}(t_1, t_0)|\psi_0\rangle.\end{aligned} \tag{50}$$
5. Before the second $\pi$-pulse at $t = t_2 - \varepsilon$, the state takes the form
$$\begin{aligned}|\Psi(t_2 - \varepsilon)\rangle &= \hat{U}_a(t_2, t_1)|\Psi(t_1 + \varepsilon)\rangle \\ &= -\frac{i}{\sqrt{2}}e^{-i\phi_\mathrm{L}(t_1)}|g_2\rangle\hat{U}_{a_2}(t_2, t_1)\hat{U}_{a_1}(t_1, t_0)|\psi_0\rangle \\ &\quad - \frac{1}{\sqrt{2}}e^{-i[\phi_\mathrm{L}(t_0)-\phi_\mathrm{L}(t_1)]}|g_1\rangle\hat{U}_{a_1}(t_2, t_1)\hat{U}_{a_2}(t_1, t_0)|\psi_0\rangle.\end{aligned} \tag{51}$$
6. After the second $\pi$-pulse at $t = t_2 + \varepsilon$, we arrive at the state
$$\begin{aligned}|\Psi(t_2 + \varepsilon)\rangle &= \hat{U}_\mathrm{p}\left(\frac{\pi}{2}\right)|\Psi(t_2 - \varepsilon)\rangle \\ &= -\frac{1}{\sqrt{2}}e^{-i[\phi_\mathrm{L}(t_1)-\phi_\mathrm{L}(t_2)]}|g_1\rangle\hat{U}_{a_2}(t_2, t_1)\hat{U}_{a_1}(t_1, t_0)|\psi_0\rangle \\ &\quad + \frac{i}{\sqrt{2}}e^{-i[\phi_\mathrm{L}(t_0)-\phi_\mathrm{L}(t_1)+\phi_\mathrm{L}(t_2)]} \\ &\quad \times |g_2\rangle\hat{U}_{a_1}(t_2, t_1)\hat{U}_{a_2}(t_1, t_0)|\psi_0\rangle.\end{aligned} \tag{52}$$
7. Before the second $\frac{\pi}{2}$-pulse at $t = t_3 - \varepsilon$, the state reads
$$\begin{aligned}|\Psi(t_3 - \varepsilon)\rangle &= \hat{U}_a(t_3, t_2)|\Psi(t_2 + \varepsilon)\rangle \\ &= -\frac{1}{\sqrt{2}}e^{-i[\phi_\mathrm{L}(t_1)-\phi_\mathrm{L}(t_2)]} \\ &\quad \times |g_1\rangle\hat{U}_{a_1}(t_3, t_2)\hat{U}_{a_2}(t_2, t_1)\hat{U}_{a_1}(t_1, t_0)|\psi_0\rangle \\ &\quad + \frac{i}{\sqrt{2}}e^{-i[\phi_\mathrm{L}(t_0)-\phi_\mathrm{L}(t_1)+\phi_\mathrm{L}(t_2)]} \\ &\quad \times |g_2\rangle\hat{U}_{a_2}(t_3, t_2)\hat{U}_{a_1}(t_2, t_1)\hat{U}_{a_2}(t_1, t_0)|\psi_0\rangle.\end{aligned} \tag{53}$$
8. Finally, after the second $\frac{\pi}{2}$-pulse at $t = t_3 + \varepsilon$, we conclude with the state
$$\begin{aligned}|\Psi(t_3 + \varepsilon)\rangle &= \hat{U}_\mathrm{p}\left(\frac{\pi}{4}\right)|\Psi(t_3 - \varepsilon)\rangle \\ &= \frac{1}{2}e^{-i[\phi_\mathrm{L}(t_1)-\phi_\mathrm{L}(t_2)]}|g_1\rangle\big(e^{-i\varphi_\mathrm{L}}\hat{U}_\mathrm{u} - \hat{U}_\mathrm{l}\big)|\psi_0\rangle \\ &\quad + \frac{i}{2}e^{-i[\phi_\mathrm{L}(t_1)-\phi_\mathrm{L}(t_2)+\phi_\mathrm{L}(t_3)]}|g_2\rangle\big(e^{-i\varphi_\mathrm{L}}\hat{U}_\mathrm{u} + \hat{U}_\mathrm{l}\big)|\psi_0\rangle,\end{aligned} \tag{54}$$
where
$$\hat{U}_\mathrm{l} \equiv \hat{U}_{a_1}(t_3, t_2)\hat{U}_{a_2}(t_2, t_1)\hat{U}_{a_1}(t_1, t_0)$$
and
$$\hat{U}_\mathrm{u} \equiv \hat{U}_{a_2}(t_3, t_2)\hat{U}_{a_1}(t_2, t_1)\hat{U}_{a_2}(t_1, t_0) \tag{55}$$
are the unitary evolution operators associated with the center-of-mass motion for the lower and the upper paths of the interferometer shown in Fig. 2, and
$$\varphi_\mathrm{L} \equiv \phi_\mathrm{L}(t_0) - 2\phi_\mathrm{L}(t_1) + 2\phi_\mathrm{L}(t_2) - \phi_\mathrm{L}(t_3) \tag{56}$$
is the total phase resulting from the action of the four laser pulses.

## Appendix D: Conditions for a closed $T^3$ -interferometer

In the preceding Appendix, we have derived an expression for the complete quantum state of the atom in the exit ports of the interferometer. Here we have allowed arbitrary times for the interactions with the laser pulses. In the present Appendix, we choose these times in such a way as to maximize the contrast.

The probability $P_{g_1}$ to observe atoms in the ground state $|g_1\rangle$ after the action of the four Raman pulses at $t = t_3 + \varepsilon$, follows from the quantum state $|\Psi(t_3 + \varepsilon)\rangle$ given by Eq. (54) and contains the state
$$|\psi_{g_1}\rangle \equiv \langle g_1|\Psi(t_3 + \varepsilon)\rangle \tag{57}$$

of the center-of-mass motion of atom in $|g_1\rangle$. It takes the form

$$P_{g_1} \equiv \langle \psi_{g_1} | \psi_{g_1} \rangle = \frac{1}{2}\left[1 - C\cos\left(\varphi_\mathrm{i} + \varphi_\mathrm{L}\right)\right], \quad (58)$$

where the contrast $C$ and the phase $\varphi_\mathrm{i}$ of the interferometer are the modulus and the argument of the matrix element

$$\langle \psi_0 | \hat{U}_\mathrm{u}^\dagger \hat{U}_\mathrm{l} | \psi_0 \rangle \equiv C e^{i\varphi_\mathrm{i}}. \quad (59)$$

We maximize $C$, that is we have $C = 1$, when we close our interferometer. In this case $P_{g_1}$ given by Eq. (58) is independent of the initial velocity and position of the atom.

To close the interferometer we have to find the time intervals $t_{j+1,j} \equiv t_{j+1} - t_j$ with $j = 0, 1, 2$ between the Raman pulses shown in Fig. 2, such that the final velocities $v_\mathrm{u}(t_3)$ and $v_\mathrm{l}(t_3)$, as well as the final positions $z_\mathrm{u}(t_3)$ and $z_\mathrm{l}(t_3)$ on the upper and lower paths of the interferometer are identical.

Indeed, for the velocity we derive the following formulae:

(i) for the upper path

$$\begin{aligned} v_0 &\to v_\mathrm{u}(t_1) = v_0 + a_2 t_{10} \\ &\to v_\mathrm{u}(t_2) = v_\mathrm{u}(t_1) + a_1 t_{21} \\ &\to v_\mathrm{u}(t_3) = v_\mathrm{u}(t_2) + a_2 t_{32} \end{aligned}$$

(ii) for the lower path

$$\begin{aligned} v_0 &\to v_\mathrm{l}(t_1) = v_0 + a_1 t_{10} \\ &\to v_\mathrm{l}(t_2) = v_\mathrm{l}(t_1) + a_2 t_{21} \\ &\to v_\mathrm{l}(t_3) = v_\mathrm{l}(t_2) + a_1 t_{32}. \end{aligned}$$

As a result, the interferometer is closed in *velocity* space, if $v_\mathrm{u}(t_3) = v_\mathrm{l}(t_3)$, that is,

$$\begin{aligned} &v_0 + a_2 t_{10} + a_1 t_{21} + a_2 t_{32} \\ &= v_0 + a_1 t_{10} + a_2 t_{21} + a_1 t_{32}, \end{aligned}$$

or, equivalently,

$$t_{10} - t_{21} + t_{32} = 0. \quad (60)$$

As for the position, we obtain the following rather lengthy expressions:

(i) for the upper path

$$\begin{aligned} z_0 &\to z_\mathrm{u}(t_1) = z_0 + v_0 t_{10} + \frac{1}{2} a_2 t_{10}^2 \\ &\to z_\mathrm{u}(t_2) = z_\mathrm{u}(t_1) + v_\mathrm{u}(t_1) t_{21} + \frac{1}{2} a_1 t_{21}^2 \\ &\to z_\mathrm{u}(t_3) = z_\mathrm{u}(t_2) + v_\mathrm{u}(t_2) t_{32} + \frac{1}{2} a_2 t_{32}^2 \\ &= z_0 + v_0(t_{10} + t_{21} + t_{32}) + \frac{1}{2}(a_2 t_{10}^2 + a_1 t_{21}^2 + a_2 t_{32}^2) \\ &\quad + a_2 t_{10}(t_{21} + t_{32}) + a_1 t_{21} t_{32}, \end{aligned}$$

(ii) for the lower path

$$\begin{aligned} z_0 &\to z_\mathrm{l}(t_1) = z_0 + v_0 t_{10} + \frac{1}{2} a_1 t_{10}^2 \\ &\to z_\mathrm{l}(t_2) = z_\mathrm{l}(t_1) + v_\mathrm{l}(t_1) t_{21} + \frac{1}{2} a_2 t_{21}^2 \\ &\to z_\mathrm{l}(t_3) = z_\mathrm{l}(t_2) + v_\mathrm{l}(t_2) t_{32} + \frac{1}{2} a_1 t_{32}^2 \\ &= z_0 + v_0(t_{10} + t_{21} + t_{32}) + \frac{1}{2}(a_1 t_{10}^2 + a_2 t_{21}^2 + a_1 t_{32}^2) \\ &\quad + a_1 t_{10}(t_{21} + t_{32}) + a_2 t_{21} t_{32}. \end{aligned}$$

As a result, the interferometer is closed in *position* space if $z_\mathrm{u}(t_3) = z_\mathrm{l}(t_3)$, that is,

$$t_{10}^2 - t_{21}^2 + t_{32}^2 + 2t_{10}(t_{21} + t_{32}) - 2t_{21}t_{32} = 0. \quad (61)$$

When we solve the system of the two algebraic Eqs. (60) and (61), for $t_{21}$ and $t_{32}$ in terms of $t_{10}$, we obtain

$$t_3 - t_2 = t_1 - t_0 = T \quad \text{and} \quad t_2 - t_1 = 2T. \quad (62)$$

Hence, to close the interferometer, the four Raman pulses must be separated in time by $T$, $2T$, and $T$ as indicated in Fig. 2.

## Appemdix E: Interferometer phase

In the preceding Appendix, we have used classical trajectories to find the separation $T - 2T - T$ between the four Raman pulses leading to a closed interferometer. We now show that in this case the product $\hat{U}_\mathrm{u}^\dagger \hat{U}_\mathrm{l}$ of the evolution operators $\hat{U}_\mathrm{l}$ and $\hat{U}_\mathrm{u}$ defined by Eq. (55) is proportional [28, 37, 67] to the identity operator, that is

$$\hat{U}_\mathrm{u}^\dagger \hat{U}_\mathrm{l} = e^{i\varphi_\mathrm{i}}\, 1, \quad (63)$$

where $\varphi_\mathrm{i}$ is the interferometer phase.

Therefore, a normalized state $|\psi_0\rangle$ leads by virtue of Eq. (59) to a perfect contrast, that is $C = 1$, indicating that the interferometer is independent of $|\psi_0\rangle$. Moreover, this calculation provides us with an explicit expression for $\varphi_\mathrm{i}$.

To evaluate the evolution operator

$$\hat{U}_\mathrm{l} \equiv \hat{U}_{a_1}(T)\hat{U}_{a_2}(2T)\hat{U}_{a_1}(T) \quad (64)$$

for the lower path of our interferometer, shown in Fig. 2, we use the Baker–Campbell–Hausdorff and Zassenhaus formulas [85] to represent the operator $\hat{U}_a(T)$ given by Eq. (13) in the form of a product

$$\hat{U}_a(T) = \exp\left(i\frac{ma^2T^3}{12\hbar}\right)\hat{\mathcal{D}}\left(\frac{1}{2}aT^2, maT\right)\hat{U}_0(T) \quad (65)$$

consisting of a phase factor, the displacement operator

$$\hat{\mathcal{D}}(Z,P) \equiv \exp\left[-\frac{i}{\hbar}\left(Z\hat{p}_z - P\hat{z}\right)\right], \tag{66}$$

and the unitary operator

$$\hat{U}_0(T) \equiv \exp\left(-\frac{i}{\hbar}\frac{\hat{p}_z^2}{2m}T\right) \tag{67}$$

of a free particle.

The decomposition, Eq. (65), allows us to rewrite Eq. (64) as

$$\hat{U}_1 = \exp\left[i\frac{m(a_1^2+4a_2^2)}{6\hbar}T^3\right]\hat{\mathcal{D}}\left(\frac{1}{2}a_1T^2, ma_1T\right)\hat{U}_0(T) \\ \times \hat{\mathcal{D}}\left(2a_2T^2, 2ma_2T\right)\hat{U}_0(2T)\hat{\mathcal{D}}\left(\frac{1}{2}a_1T^2, ma_1T\right)\hat{U}_0(T). \tag{68}$$

With the help of the commutation relation

$$\hat{U}_0(T)\hat{\mathcal{D}}(Z,P) = \hat{\mathcal{D}}\left(Z + \frac{P}{m}T, P\right)\hat{U}_0(T)$$

and the addition identity

$$\hat{U}_0(T_1)\hat{U}_0(T_2) = \hat{U}_0(T_1+T_2)$$

for the operators $\hat{\mathcal{D}}$ and $\hat{U}$ given by Eqs. (66) and (67), we can shift all free-evolution operators $\hat{U}_0$ in Eq. (68) to the right and we arrive at

$$\hat{U}_1 = \exp\left[i\frac{m(a_1^2+4a_2^2)}{6\hbar}T^3\right]\hat{\mathcal{D}}\left(\frac{1}{2}a_1T^2, ma_1T\right)$$

$$\times\hat{\mathcal{D}}\left(4a_2T^2, 2ma_2T\right)\hat{\mathcal{D}}\left(\frac{7}{2}a_1T^2, ma_1T\right)\hat{U}_0(4T),$$

or

$$\hat{U}_1 = \exp\left[i\frac{mT^3}{3\hbar}\left(5a_1^2+9a_1a_2+2a_2^2\right)\right] \\ \times \hat{\mathcal{D}}\left(4(a_1+a_2)T^2, 2m(a_1+a_2)T\right)\hat{U}_0(4T). \tag{69}$$

In the last step we have made use of the addition identity

$$\hat{\mathcal{D}}\left(Z_1,P_1\right)\hat{\mathcal{D}}\left(Z_2,P_2\right) = e^{i\tilde{\varphi}}\hat{\mathcal{D}}\left(Z_1+Z_2, P_1+P_2\right)$$

with

$$\tilde{\varphi} \equiv \frac{1}{2\hbar}\left(P_1Z_2 - P_2Z_1\right),$$

to combine all three displacement operators into a single one.

Since the evolution operator $\hat{U}_\mathrm{u}$ defined by Eq. (55) for the upper path of our interferometer follows directly from the operator $\hat{U}_1$ given by Eq. (69) for the lower path by an exchange of the accelerations $a_1$ and $a_2$, we arrive at

$$\hat{U}_\mathrm{u} = \exp\left[i\frac{mT^3}{3\hbar}\left(2a_1^2+9a_1a_2+5a_2^2\right)\right]$$

$$\times\hat{\mathcal{D}}\left(4(a_1+a_2)T^2, 2m(a_1+a_2)T\right)\hat{U}_0(4T). \tag{70}$$

When we substitute Eqs. (69) and (70) into the left-hand side of Eq. (63) and use the property that the operators $\hat{\mathcal{D}}$ and $\hat{U}_0$ are unitary, the interferometer phase reads

$$\varphi_\mathrm{i} = \frac{m}{\hbar}\left(a_1^2 - a_2^2\right)T^3. \tag{71}$$

Hence, $\varphi_\mathrm{i}$ is independent of the initial position $z_0$ and velocity $v_0$ as well as of the initial state. Moreover, it scales with the third power of the time interval $T \equiv t_1 - t_0$ between the first and the second Raman pulses.

## References


1. S. Fray, C. Alvarez Diez, Th.W. Hänsch, M. Weitz, Phys. Rev. Lett. **93**, 240404 (2004)
2. E.H. Kennard, Zeitschrift für Physik **44**, 326 (1927)
3. E.H. Kennard, J. Frank. Inst. **207**, 47 (1929)
4. W.P. Schleich, D.M. Greenberger, D.H. Kobe, M.O. Scully, Proc. Nat. Acad. Sci. **110**, 5374 (2013)
5. P.R. Berman (ed.) *Atom Interferometry* (Academic Press, San Diego, 1997)
6. A.D. Cronin, J. Schmiedmayer, D.E. Pritchard, Rev. Mod. Phys. **81**, 1051 (2009)
7. G.M. Tino, M.A. Kasevich (eds.) Proceedings of the International School of Physics "Enrico Fermi" Course 188 "Atom Interferometry" (IOS, Amsterdam, 2014)
8. R.P. Feynman, A.R. Hibbs, *Quantum Mechanics and Path Integrals* (McGraw-Hill, New York, 1965)
9. M.V. Berry, J. Phys. A **15**, L385 (1982)
10. F. Fratini, L. Safari, Physica Scripta **89**, 085004 (2014)
11. P. Storey, C. Cohen-Tannoudji, J. Phys. II **4**, 1999 (1994)
12. G.D. McDonald, C.C.N. Kuhn, S. Bennetts, J.E. Debs, K.S. Hardman, J.D. Close, N.P. Robins, EPL **105**, 63001 (2014)
13. G.D. McDonald, C.C.N. Kuhn, arXiv:1312.2713 (2013)
14. Ch.J. Bordé, Ch. Salomon, S. Avrillier, A. van Lerberghe, Ch. Bréant, D. Bassi, G. Scoles, Phys. Rev. A **30**, 1836 (1984)
15. Ch.J. Bordé, Phys. Lett. A **140**, 10 (1989)
16. J.F. Clauser, Physica B **151**, 262 (1988)
17. K.-P. Marzlin, J. Audretsch, Phys. Rev. A **53**, 312 (1996)
18. T.L. Gustavson, *Precision rotation sensing using atom interferometry*, Ph.D. thesis, (Stanford University, 2000)
19. J.M. McGuirk, G.T. Foster, J.B. Fixler, M.J. Snadden, M.A. Kasevich, Phys. Rev. A **65**, 033608 (2002)
20. F.Y. Leduc, *Caractérisation d'un capteur inertiel à atomes froids*, Ph.D. thesis, (Université Paris XI Orsay, 2004)
21. B. Canuel, F. Leduc, D. Holleville, A. Gauguet, J. Fils, A. Virdis, A. Clairon, N. Dimarcq, Ch.J. Bordé, A. Landragin, P. Bouyer, Phys. Rev. Lett. **97**, 010402 (2006)
22. B. Dubetsky, M.A. Kasevich, Phys. Rev. A **74**, 023615 (2006)
23. A. Tonyushkin, M. Prentiss, Phys. Rev. A **78**, 053625 (2008)
24. S. Wu, E. Su, M. Prentiss, Phys. Rev. Lett. **99**, 173201 (2007)
25. K. Takase, *Precision rotation rate measurements with a mobile atom interferometer*, Ph.D. thesis, (Stanford University, 2008)

26. T. Lévèque, *Développement d'un gyromètre à atomes froids de haute sensibilité fondé sur une géométrie repliée*, Ph.D. thesis, (Observatoire de Paris, 2010)
27. J.K. Stockton, K. Takase, M.A. Kasevich, Phys. Rev. Lett. **107**, 133001 (2011)
28. S. Kleinert, E. Kajari, A. Roura, W.P. Schleich, Phys. Rep. **605**, 1 (2015)
29. J. Audretsch, K.-P. Marzlin, J. Phys. II **4**, 2073 (1994)
30. P. Wolf, P. Tourrenc, Phys. Lett. A **251**, 241 (1999)
31. A. Peters, K.Y. Chung, S. Chu, Metrologia **38**, 25 (2001)
32. Ch.J. Bordé, Eur. Phys. J. Spec. Top. **163**, 315 (2008)
33. H. Rauch, S.A. Werner, *Neutron Interferometry*, 2nd edn. (Oxford University Press, New York, 2015)
34. D.M. Greenberger, W.P. Schleich, E.M. Rasel, Phys. Rev. A **86**, 063622 (2012)
35. W.P. Schleich, D.M. Greenberger, E.M. Rasel, Phys. Rev. Lett. **110**, 010401 (2013)
36. W.P. Schleich, D.M. Greenberger, E.M. Rasel, New J. Phys. **15**, 013007 (2013)
37. A. Roura, W. Zeller, W.P. Schleich, New J. Phys. **16**, 123012 (2014)
38. W. Zeller, *The impact of wave-packet dynamics in long-time atom interferometry*, PhD thesis, (Ulm University, 2016)
39. C. Misner, K. Thorne, J.A. Wheeler, *Gravitation* (W. H. Freeman, San Francisco, 1973)
40. D. Bohm, *Quantum Theory* (Prentice Hall, Englewood Cliffs, 1951)
41. N. Bohr, L. Rosenfeld, Kgl. Danske Videnskab. Selskab, Mat.-fys. Medd. **12,** No. 8 (1933)
42. N. Bohr, L. Rosenfeld, Phys. Rev. **78**, 794 (1950)
43. H. Salecker, E.P. Wigner, Phys. Rev. **109**, 571 (1958)
44. J.A. Wheeler, in Proceedings of the International School of Physics "Enrico Fermi" Course 72 "Problems in the foundations of physics" (North-Holland, Amsterdam, 1979)
45. C.M. DeWitt, D. Rickle (eds.) *Conference on the Role of Gravitation in Physics*, (Wright Air Development Center, 1957). These proceedings have been reprinted under the title *The Role of Gravitation in Physics* by the Max-Planck Research Library for the History and Development of Knowledge
46. D.M. Greenberger, J. Math. Phys. **11,** 2329 (1970); *ibid.***11,** 2341 (1970)
47. R. Colella, A.W. Overhauser, S.A. Werner, Phys. Rev. Lett. **34**, 1472 (1975)
48. J.-L. Staudenmann, S.A. Werner, R. Colella, A.W. Overhauser, Phys. Rev. A **21**, 1419 (1980)
49. K.C. Littrell, B.E. Allman, S.A. Werner, Phys. Rev A **56**, 1767 (1997)
50. K. Hornberger, S. Gerlich, P. Haslinger, S. Nimmrichter, M. Arndt, Rev. Mod. Phys. **84**, 157 (2012)
51. E.A. Cornell, C.E. Wieman, Rev. Mod. Phys. **74**, 875 (2002)
52. W. Ketterle, Rev. Mod. Phys. **74**, 1131 (2002)
53. D. Schlippert, J. Hartwig, H. Albers, L.L. Richardson, C. Schubert, A. Roura, W.P. Schleich, W. Ertmer, E.M. Rasel, Phys. Rev. Lett. **112**, 203002 (2014)
54. S. Dimopoulos, P.W. Graham, J.M. Hogan, M.A. Kasevich, Phys. Rev. D **78**, 042003 (2008)
55. I. Pikovski, M. Zych, F. Costa, Č. Brukner, Nat. Phys. **11**, 668 (2015)
56. M. Köhl, Th.W. Hänsch, T. Esslinger, Phys. Rev. Lett. **87**, 160404 (2001)
57. C.W. Chou, D.B. Hume, T. Rosenband, D.J. Wineland, Science **329**, 1630 (2010)
58. A. Matveev, Ch.G. Parthey, K. Predehl, J. Alnis, A. Beyer, R. Holzwarth, Th. Udem, T. Wilken, N. Kolachevsky, M. Abgrall, D. Rovera, Ch. Salomon, Ph. Laurent, G. Grosche, O. Terra, Th. Legero, H. Schnatz, S. Weyers, B. Altschul , Th.W. Hänsch, Phys. Rev. Lett. **110**, 230801 (2013)
59. T. Jenke, P. Geltenbort, H. Lemmel, H. Abele, Nat. Phys. **7**, 468 (2011)
60. H. Abele, H. Leeb, New J. Phys. **14**, 055010 (2012)
61. T. Jenke, G. Cronenberg, J. Burgdörfer, L.A. Chizhova, P. Geltenbort, A.N. Ivanov, T. Lauer, T. Lins, S. Rotter, H. Saul, U. Schmidt, H. Abele, Phys. Rev. Lett. **112**, 151105 (2014)
62. C. Kiefer, *Quantum Gravity* (Oxford University Press, Oxford, 2007)
63. S. Abend, M. Gebbe, M. Gersemann, H. Ahlers, H. Müntinga, E. Giese, N. Gaaloul, C. Schubert, C. Lämmerzahl, W. Ertmer, W.P. Schleich, E.M. Rasel, Phys. Rev. Lett. **117**, 203003 (2016)
64. M.A. Kasevich, S. Chu, Phys. Rev. Lett. **67**, 181 (1991)
65. M.A. Kasevich, S. Chu, Appl. Phys. B **54**, 321 (1992)
66. E. Kajari, N.L. Harshman, E.M. Rasel, S. Stenholm, G. Süssmann, W.P. Schleich, Appl. Phys. B **100**, 43 (2010)
67. E. Giese, W. Zeller, S. Kleinert, M. Meister, V. Tamma, A. Roura, W.P. Schleich, Proceedings of the International School of Physics "Enrico Fermi" Course 188 "Atom Interferometry", ed. by G.M. Tino, M.A. Kasevich (IOS, Amsterdam, 2014)
68. D.M. Greenberger, Phys. Rev. Lett **87**, 100405 (2001)
69. J. Schmiedmayer, Ch. Ekstrom, M. Chapman, T. Hammond, D. Pritchard, J. Phys. II **4**, 2029 (1994)
70. M. Jacquey, A. Miffre, M. Büchner, G. Trénec, J. Vigué, EPL **77**, 20007 (2007)
71. D.A. Steck, Rubidium 85 D Line Data. http://steck.us/alkalidata (revision 2.1.6, 20 September 2013)
72. J.M. Hogan, D.M.S. Johnson, M.A. Kasevich, in Proceedings of the International School of Physics "Enrico Fermi" on Atom Optics and Space Physics, ed. by E. Arimondo, W. Ertmer, and W.P. Schleich (Amsterdam, 2009)
73. G.D. McDonald, C.C.N. Kuhn, S. Bennetts, J.E. Debs, K.S. Hardman, M. Johnsson, J.D. Close, N.P. Robins, Phys. Rev. A **88**, 053620 (2013)
74. S. Chiow, T. Kovachy, H. Chien, M.A. Kasevich, Phys. Rev. Lett. **107**, 130403 (2011)
75. A. Roura. arXiv:1509.08098 (2015)
76. S.A. DeSavage, J.P. Davis, F.A. Narducci, J. Mod. Opt. **60**, 95 (2013)
77. S.A. DeSavage, K.H. Gordon, E.M. Clifton, J.P. Davis, F.A. Narducci, J. Mod. Opt. **58**, 2028 (2011)
78. C.L. Adler, R. Johnson, A. Srinivasan, F.A. Narducci, to be submitted (2016)
79. G. Breit, Phys. Rev. **32**, 273 (1928)
80. M.V. Berry, N.L. Balazs, Am. J. Phys. **47**, 264 (1979)
81. W.P. Schleich, *Quantum Optics in Phase Space* (Wiley-VCH, Weinheim, 2001)
82. Y.N. Demkov, V.D. Kondratovich, V.N. Ostrovskii, Pis'ma Zh. Eksp. Teor. Fiz. **34**, 425 (1981)
83. C. Bracher, T. Kramer, M. Kleber, Phys. Rev. A **67**, 043601 (2003)
84. C. Blondel, C. Delsart, F. Dulieu, Phys. Rev. Lett. **77**, 3755 (1996)
85. R.M. Wilcox, J. Math. Phys. **8**, 962 (1967)